UNIVERSITY
OF TRENTO

DIPARTIMENTO DI INGEGNERIA E SCIENZA DELL'INFORMAZIONE

38123 Povo – Trento (Italy), Via Sommarive 14
http://www.disi.unitn.it

VALIDATION OF A SMART ANTENNA PROTOTYPE: MODEL AND EXPERIMENTS

M. Benedetti, G. Oliveri, and A. Massa

January 2011

Technical Report # DISI-11-181

Validation of a Smart Antenna Prototype: Model and Experiments

Manuel Benedetti, Giacomo Oliveri, and Andrea Massa [1]

ELEDIA Group - Department of Information Engineering and Computer Science
University of Trento, Via Sommarive 14, I-38050 Trento, Italy
[1]andrea.massa@ing.unitn.it

Abstract

In this paper, the architecture of a smart antenna prototype is described and its functionality assessed. The system prototype is composed by an 8-elements linear array of dipoles with a finite reflecting plane and the adaptive behavior is obtained modifying a set of array weights with electronically-driven vector modulators. In order to real-time react to complex interference scenarios, the system is controlled by a software control module based on a Particle Swarm Optimizer. To demonstrate the feasibility and the effectiveness of the proposed implementation, a set of representative results concerned with realistic interference scenarios is reported and discussed.

I. Introduction

Thanks to the development of wireless technologies, mobile communication devices have known a wide diffusion in the last decade. To properly deal with complex scenarios characterized by multiple users as well as different standards, communication systems that allow a suitable quality of service (QoS) and an enhanced security are needed [1]. In this framework, smart antennas [2] have been recognized as promising tools for an efficient management of the physical layer. Such systems usually consist of an antenna array and a signal processing module to real-time maximize the quality of the communication evaluated (at the physical layer) in terms of signal-to-interference-plus-noise ratio (*SINR*) at the receiver. Towards this end, smart antennas steer the main lobe of the beam pattern to track the desired signal and cancel the interferences determining suitable attenuation values along the jammers directions.

Although the effectiveness of a hardware implementation has been theoretically proved [3], the technological difficulties and costs for the implementation of fully-adaptive solutions prevented a widespread application of smart antennas in wireless communications. As a matter of fact, simpler architectures have been usually considered. As far as parasitic architectures are concerned, several prototypes have been implemented by exploiting the theoretical basis of the functioning of the Uda-Yagi antennas [4] (i.e., a single active antenna whose pattern is shaped by means of a set of real-time controlled parasitic elements). Despite compact sizes and low-cost architectures, such devices are not able to steer the position of the pattern nulls in a continuous way, thus limiting the adaptation to the environment of the whole transmission system.

Consequently, some efforts have been devoted to realize a fully-adaptive behavior and more complex prototypes have been built. Some devices have been implemented making use of complex acquisition systems, where the signal is collected at the receiver and at the output of the array elements in order to compute the co-variance matrix [5][6]. On the other hand, simpler fully-adaptive systems based on the measurement of the received signal at the receiver have been also implemented [7]. Such devices are usually controlled by means of heuristic optimization strategies aimed at maximizing a suitable fitness function proportional to the signal-to-interference-plus-noise ratio. In both cases, the effectiveness of the implementation has been assessed by comparing measured and simulated radiation patterns in correspondence with a single interferer incoming from a fixed direction.

This paper discusses the implementation of a fully-adaptive smart antenna preliminarily assessed in [8] and focus on the experimental validation by considering complex interference scenarios. The prototype is characterized by a simple functional scheme where the signals collected by the array elements are suitably weighted by the hardware control unit according to an

iterative strategy based on a customized version of the Particle Swarm Optimizer (PSO) [9] to maximize a suitable fitness function. As far as the validation is concerned, an experiment characterized by multiple slots of time and different directions of arrival for the interferences is considered. The efficiency of the proposed implementation is analyzed in terms of both the behavior of the signal-to-interference-plus-noise (*SINR*) ratio and the capability of placing nulls in suitable positions of the radiation pattern.

II. Smart Antenna Behavior

Let us consider a linear array of M equally-spaced elements. At each time-step[1] t_l, $l = 1, ..., L$, the antenna receives a signal from a desired source and a set of Q interfering sources. The signal collected at the m-th element of the array is given by

$$s_m(t_l) = d_m(t_l) + \sum_{q=1}^{Q} u_{q,m}(t_l) + n_m(t_l) \qquad m = 1, ..., M \tag{1}$$

where d_m and $u_{q,m}$ denote the contribution of the desired signal and of the q-th interference, $q = 1, ..., Q$, respectively. Moreover, n_m models the uncorrelated background noise. The signal $y(t_l)$ available at the output of the receiver turns out to be

$$y(t_l) = \sum_{m=1}^{M} w_m(t_l)\, s_m(t_l) \tag{2}$$

where $w_m(t_l) = \alpha_m(t_l)\, e^{j\beta_m(t_l)}$ is the m-th complex weight at the l-th time-step.

As far as the smart behavior of the system is concerned, the weight vector $\underline{w}(t_l) = \{w_m(t_l);\, m = 1, ..., M\}$ is updated at each time-step to react to the continuously (i.e., at each time-step) changing interference/environment conditions, thus maximizing the signal-to-interference-plus-noise ratio (*SINR*) at the receiver. Since the *SINR* is not usually/easily measurable at the receiver, the total power $\Psi^{tot}(t_l)$ of the output signal $y(t_l)$ is considered [10] as an index of the system performance and the fitness function $\Theta(t_l)$

$$\Theta(t_l) = \frac{\left|\sum_{m=1}^{M} \alpha_m(t_l)\, e^{j\left[\frac{2\pi}{\lambda} x_m \cos\phi^d + \beta_m(t_l)\right]}\right|^2}{\Psi^{tot}(t_l)} \tag{3}$$

is maximized to determine the optimal weight vector $\underline{w}_{opt}(t_l) = \arg\left[\max_{\underline{w}} SINR\{\underline{w}(t_l)\}\right]$ [10]. In (3), x_m is the position of the m-th element, ϕ^d and ϕ_q^u, $q = 1, ..., Q$, are the directions of arrival (DoAs) of the desired and q-th jammer, respectively. For the sake of clarity, the measured value of Ψ^{tot} is obviously related to the array coefficients according to the following relationship

$$\Psi^{tot}(t_l) = \sum_{m=1}^{M} \alpha_m(t_l)\, e^{j\beta_m(t_l)} \sum_{i=1}^{M} \alpha_i(t_l)\, e^{-j\beta_i(t_l)} \Omega_{i,m}^{tot} \tag{4}$$

where $\Omega_{i,m}^{tot}$ is the (i, m)-th entry of the co-variance matrix of the received signal $y(t_l)$ [11].

At each time-step, the arising optimization problem

$$\underline{w}_{opt}(t_l) = \arg\left[\max_{\underline{w}} \Theta\{\underline{w}(t_l)\}\right] \tag{5}$$

is then solved by means of a PSO-driven approach following the implementation guidelines in [9]. More specifically, a swarm of P particles is used to model the trial solutions at each time-step. The swarm samples the solution space in a set of successive iterations, $k_l = 1, ..., K_{max}$ (k_l being the iteration index of the l-th time-step) by exploiting the history of the swarm as well as the knowledge of the optimal solutions at the previous steps (i.e., the so-called *swarm memory* $\Pi(t_l) = \left\{\underline{w}_{opt}(t_i),\, i = l-1, l-2, ...\right\}$) until the new time-step ($l \leftarrow l+1$) or when $\Theta\{\underline{w}(t_l)\} \geq \eta$, η being a user-defined convergence threshold.

[1] A time-step is a slot of time, between two consecutive snapshots, characterized by the presence of a desired signal and a fixed number of interfering signals with invariant directions of arrival (DoAs).

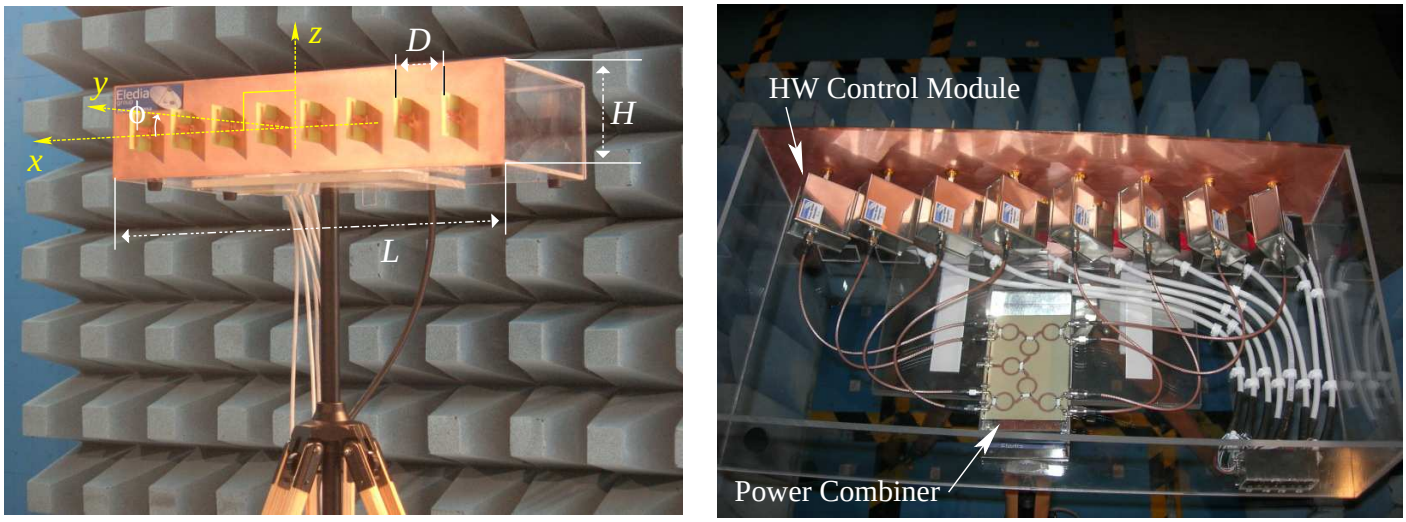

(*a*) (*b*)

Fig. 1. Photographs of the Fully-Adaptive Smart Antenna prototype: (*a*) Front view (*Radiating Module*) and (*b*) back view (*HW Control Module* and *Power Combiner*).

III. Architecture of the Smart Antenna

The smart antenna prototype operates as a receiving system in the *ISM* band ($f_c = 2.45\,GHz$). It is composed by the following functional blocks: (*a*) a "Radiating Module" [Fig. 1(*a*)]; (*b*) a "Hardware Control Module" [Fig. 1(*b*)]; (*c*) a "Radio-frequency Signals Combiner"; and (*d*) a "Software Control Module" [8]. More specifically, the architecture of the functional blocks is described in the following subsections.

A. Radiating Module

The array consists of $M = 8$ ($D = \frac{\lambda}{2}$ being the inter-element distance where λ is the free-space wavelength) printed dipoles built following the indications given in [12]. More specifically, the ground plane of the feeding microstrip line and the half-wave dipole strips have been printed on the same plane, while the via-hole balun has been placed on the other side of the FR-4 substrate. With reference to Fig. 1(*a*), a finite reflecting plane of length $L = 4.5\,\lambda$ and height $H = \lambda$ has been placed behind and parallel to the dipoles at a distance $W = 0.25\,\lambda$ from their arms.

B. Hardware Control Module

The HW Control Module is composed by a set of M AD8341 Analog Device RF vector modulators [13] that weight the signals $s_m(k_l)$, $m = 1, ..., M$, from the array elements with the coefficients $w_m(k_l)$, $m = 1, ..., M$, computed by the PSO-driven control. Such a module has been installed on a FR-4 printed circuit board (PCB) and each modulator is driven by two low-frequency differential signals $\nu_m(k_l)$, $\zeta_m(k_l) \in [-0.5,\, 0.5\,V]$ to generate a phase shift value β_m equal to

$$\beta_m(k_l) = \arctan\frac{\nu_m(k_l)}{\zeta_m(k_l)}, \quad \beta_m \in [0°;\, 360°], \tag{6}$$

and an attenuation given by

$$\alpha_m(k_l) = \sqrt{\zeta_m(k_l)^2 + \nu_m(k_l)^2}, \quad \alpha_m \leq 0.5 \tag{7}$$

in the range $\alpha_m \in [4.5\,dB;\, 34.5\,dB]$.

C. Radio-frequency Signal Combiner

The $M = 8$ RF signals coming from the HW Control Module are added, by means of the RF power combiner shown in [Fig. 1(*b*)], to determine the output signal $y(k_l)$. The combiner is composed by seven Wilkinson devices [14] printed on an Arlon N25 substrate.

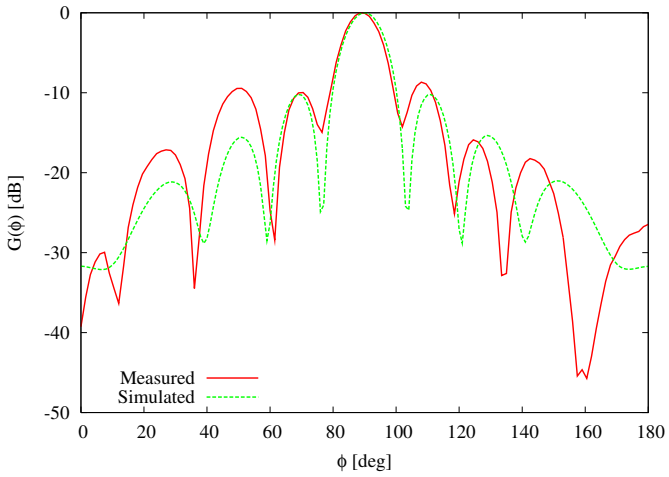

Fig. 2. *Testing Phase* - Quiescent radiation pattern.

D. PSO-driven Software Control Module

The output signal is then processed by a spectrum analyzer Agilent ESA-E4404 to measure the total output power $\Psi^{tot}(k_l)$. Such an information is then transferred to the Software (SW) Control Module by means of a GPIB input interface. Concerning the SW Control Module, it consists of a personal computer (PC) where the input/output communication interfaces and a SW unit, which implements the PSO-driven control logic [9], have been installed. At each time step t_l, the SW module maximizes the *SINR* by looking for the optimal set $\{[\zeta_m^{opt}(t_l), \nu_m^{opt}(t_l)]; m = 1, ..., M\}$ of the differential signals (i.e., the corresponding optimal weight configuration, $\underline{w}_{opt}(t_l) = \{w_m^{opt}(t_l); m = 1, ..., M\}$, being $\underline{w}_{opt}(t_l) = \arg\left[\max_{p=1,...,P}\Theta\left\{\underline{w}_p(k_l)\right\}\right]$) that optimizes (3).

IV. Experimental Validation

This section is concerned with the experimental validation of the smart antenna prototype. Firstly, the results of a preliminary testing of the prototype will be discussed. Then, the behavior of the prototype in dealing with a complex interference scenario will be described.

A. Preliminary Testing

A preliminary calibration of the prototype has been carried out by comparing, for each functional block, the numerical simulations of the design phase with a set of experimental measurements. For the sake of brevity, only the behavior of the system in a "static" configuration is discussed here.

In particular, an experiment has been carried out in order to assess the ability of the smart antenna to reproduce the simulated "quiescent" pattern. Towards this end, the radiation pattern $G(\phi)$ has been measured in a controlled environment (i.e., anechoic chamber) and it has been compared with the corresponding data from the numerical simulation, carried out by taking into account the actual structure of the antenna. Figure 2 shows the pattern generated by setting $w_m = 0.5$, $m = 1, ..., M$. As it can be observed, the simulated pattern is satisfactory matched despite some differences in the secondary lobes for $\phi < 60$ and $\phi > 130$.

B. Validation in Complex Time-Varying Scenarios

This subsection is aimed at analyzing the performance of the prototype in a time-varying situation. As far as the measurement setup is concerned, the interference sources have been placed in front of the smart antenna along a circular perimeter ($\rho = 28\,\lambda$) and at different angular positions.

The scenario is concerned with a single interference source ($Q = 1$) whose DoA and power have been varied according to the evolution detailed in Fig. 3. Moreover, ϕ^d has been set to 0° and $\Psi^d = 100\,mW$. The obtained results are summarized

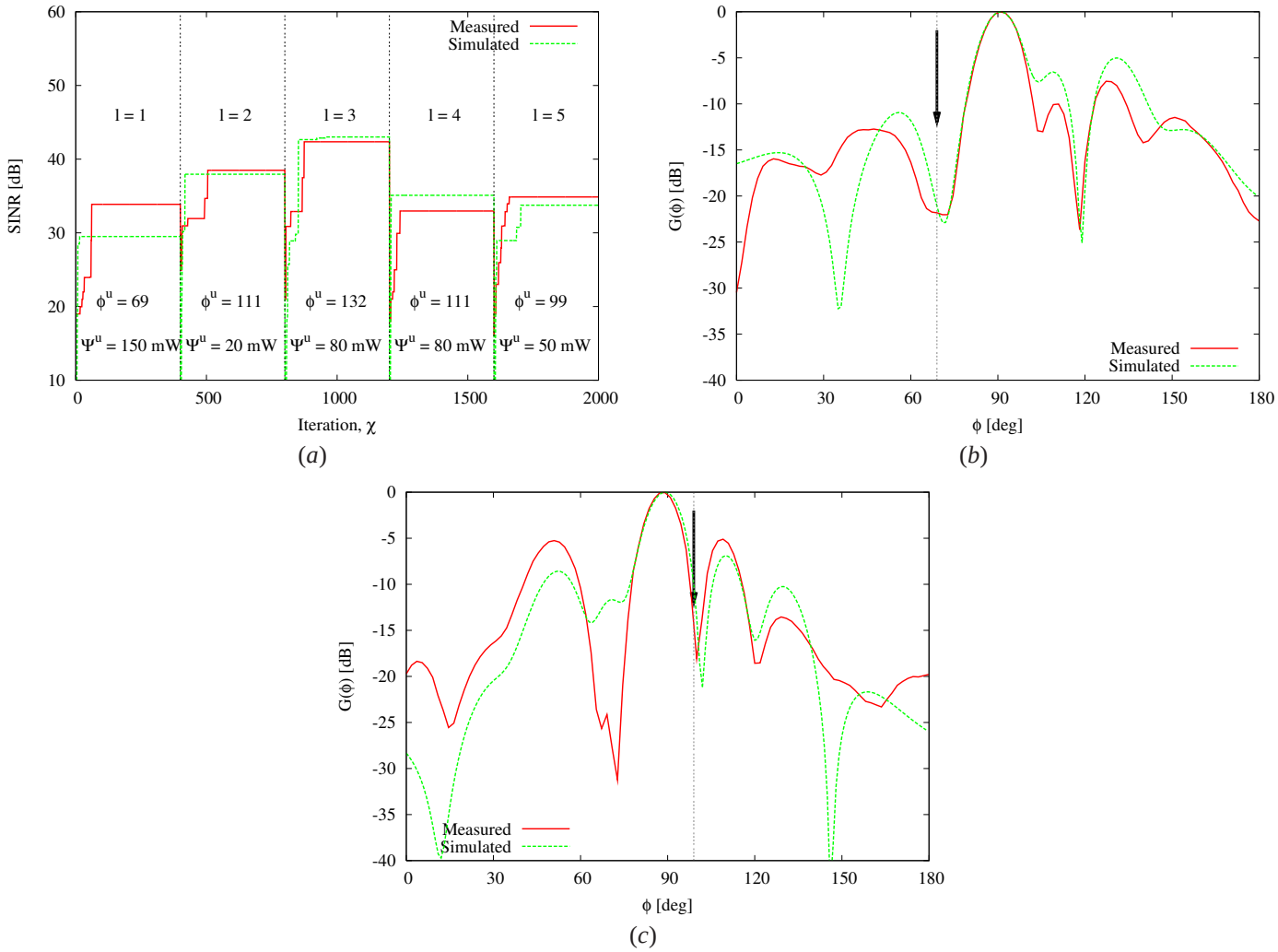

Fig. 3. *Experiment 1* - (*a*) Behavior of the *SINR* versus the iteration index χ. Beam pattern synthesized at (*b*) $l = 1$ and (c) $l = 5$.

in Fig. 3 where the behavior of the *SINR* at the receiver versus the iteration index χ ($\chi \triangleq \sum_{l=1}^{L} k_l$) [Fig. 3(*a*)] and two representative samples of the radiation pattern [Figs. 3(*b*)-3(*c*)] are reported. As for the *SINR* at each iteration χ, it has been computed as follows

$$SINR(\chi) = \frac{\tilde{\Psi}^d(\chi) - \hat{n}(\chi)}{\tilde{\Psi}^u(\chi)} \tag{8}$$

where $\tilde{\Psi}^d(\chi)$ and $\tilde{\Psi}^u(\chi)$ are the power of the desired signal and of the undesired one measured when turning off the interference sources [i.e., $u_q(\chi) = 0$, $q = 1, ..., Q$] and the desired signal [i.e., $d(\chi) = 0$], respectively. Moreover, $\hat{n}(\chi)$ is the noise level estimated at the χ-th iteration turning off both $d(\chi)$ and $u_q(\chi)$, $q = 1, ..., Q$. With reference to Fig. 3(*a*), the *SINR* values measured at each time-step t_l, $l = 1, ..., L$ turn out to be always greater than $32\,dB$ with a dynamics of about $10\,dB$ [$SINR(t_1) = 33.86\,dB$, $SINR(t_2) = 38.48\,dB$, $SINR(t_3) = 42.36\,dB$, $SINR(t_4) = 32.96\,dB$, and $SINR(t_5) = 34.86\,dB$]. For comparison purposes, the plot of the simulated *SINR* is reported, as well. As it can be observed, there is an acceptable agreement between the two plots although.

In order to give some indications of the effects of the *SINR* maximization on the antenna beamforming, some samples of the radiation pattern in correspondence with different time-steps are shown. More specifically, Figure 3(*b*) shows the pattern shape at the step $l = 1$ [$SINR(t_1) = 33.86\,dB$] when the interference impinges on the array from $\phi^u = 69°$ with a power equal to $150\,mW$. The measured beam pattern is characterized by a null of about $-22\,dB$ along the jammer direction $\phi = \phi^u$. A

similar result is obtained at $l = 5$ for a jammer coming from the direction $\phi^u = 99^\circ$ with a lower power level ($\Psi^u = 50\,mW$) [Fig. 3(*c*)].

CONCLUSIONS

In this paper, an experimental realization of a fully adaptive array has been discussed. The system is characterized by a simple architecture consisting of a radiating module, a HW control module, a power combiner, and a SW control module. The signal received at the array elements is suitably processed according to a PSO-based control strategy aimed at maximizing the SINR at the output the system. The proposed implementation is characterized by a low-complexity and low-cost architecture able to shift the locations of the pattern nulls in a continuous way. The experimental validation has demonstrated the feasibility of the adaptive control, the capability of optimizing the system performance in terms of SINR values and suppression of the interferences as well as the reliability of the antenna prototype.

REFERENCES

[1] A. Alexiou and M. Haardt, "Smart antenna technologies for future wireless systems: trends and challenges," *IEEE Comm. Mag.*, vol. 42, pp. 90-97, Sep. 2004.

[2] M. Chryssomallis, "Smart antennas," *IEEE Antennas Propag. Mag.*, vol. 42, pp. 129-136, Jun. 2000.

[3] S. P. Applebaum, "Adaptive arrays," *IEEE Trans. Antennas Propag.*, vol. 24, pp. 585-598, Sep. 1976.

[4] M. D. Migliore, D. Pinchera, and F. Schettino, "A simple and robust adaptive parasitic antenna," *IEEE Antennas Propag. Mag.*, vol. 53, pp. 3262-3272, Oct. 2005.

[5] N. Celik, W. Kim, M. F. Demirkol, M. F. Iskander, and R. Emrick, "Implementation and experimental verification of hybrid smart-antenna beamforming algorithm," *IEEE Antenna Wir. Propag. Lett.*, vol. 5, pp. 280-283, 2006.

[6] M. Diop, J.F. Diouris, and J. Saillard, "A low-cost experimental adaptive array built in the UHF band (900 MHz) for a minimum response time in interference cancellation", in *Proc. IEEE Vehicular Technology Conference*, 1992, pp. 25-28.

[7] R. L. Haupt and H. Southall, "Experimental adaptive cylindrical array," in *Proc. IEEE Aerospace Conference*, 1999, pp. 291-296.

[8] M. Benedetti, R. Azaro, and A. Massa, "Experimental validation of a fully-adaptive smart antenna prototype," *Elect. Lett.*, vol. 44, no. 11, pp. 661-662, May 2008.

[9] M. Benedetti, R. Azaro, and A. Massa, "Memory enhanced PSO-based optimization approach for smart antennas control in complex interference scenarios," *IEEE Trans. Antennas Propag.*, vol. 56, pp. 1939-1947, Jul. 2008.

[10] R. T. Compton Jr., *Adaptive Antennas*. Englewood Cliffs, NJ: Prentice Hall, 1988.

[11] L. C. Godara, *Smart Antennas*. Boca Raton, FL: CRC Press, 2004.

[12] H.-R. Chuang and L.-C. Kuo, "3-D FDTD design analysis of a 2.4-GHz polarization-diversity printed dipole antenna with integrated balun and polarization switching circuit for WLAN and wireless communication applications," *IEEE Trans. Microw. Theory Tech.*, vol. 51, pp. 374-381, Feb. 2003.

[13] Analog Devices, 2004. 1.5 GHz to 2.4 GHz RF vector modulator. One Technology Way, MA. [Online]. Available: www.analog.com/UploadedFiles/Data_Sheets/AD8341.pdf.

[14] D. M. Pozar, *Microwave Engineering*. Hoboken, NJ: John Wiley, 2005.